# Kinetics of Formation of Oil-in-Water Emulsions Using *In Situ* Rheo-Optical Measurements

**Rudy Covis, Emmanuelle Marie, and Alain Durand**
CNRS, LCPM, FRE 3564, Nancy F-54001, France

Université de Lorraine, LCPM, FRE 3564, Nancy F-54001, France

**Christophe Baravian**[†]
CNRS, LEMTA, UMR 7563, Nancy F-54001, France

Université de Lorraine, LEMTA, UMR 7563, Nancy F-54001, France

*DOI 10.1002/aic.14626*
*Published online September 23, 2014 in Wiley Online Library (wileyonlinelibrary.com)*

*The kinetics of mechanical emulsification in vane geometry was investigated using an original rheo-optic device. Hexadecane-in-water micronic emulsions were prepared using a nonionic polymeric surfactant (Brij700®) as stabilizer. The viscosity of aqueous phase was adjusted using a commercial viscosifier (Emkarox®) which ensured Newtonian behavior to the continuous phase. The influences of two variables (rotational speed and oil volume fraction) on the kinetics of droplet fragmentation were examined in detail. Rotational speed was varied between 50 and 100 rad $s^{-1}$ and had a strong effect on the kinetics of emulsion formation which was discussed on the basis of droplet fragmentation by shear forces. On the contrary, oil volume fraction (between 20 and 60% v/v) showed no marked effect, which appeared as an important result for scale-up considerations. A theoretical description of fragmentation mechanism was proposed and experimental results were compared to calculated values.* © 2014 American Institute of Chemical Engineers *AIChE J*, 61: 277–284, 2015

*Keywords: emulsification, kinetics, fragmentation, rheo-optics, laminar flow*

## Introduction

Improving performances in design and manufacture of formulated products requires better knowledge of interrelations between molecular, mesoscopic (0.1–100 μm), and macroscopic scales of soft matter.[1–3] This question is a current scientific challenge for both industrial and academic research. Emulsions represent a significant part of formulated products finding applications in very different domains.[4] A lot of work addressed the control of emulsion characteristics like droplet diameter distribution, colloidal stability, or ageing with stabilizers like macromolecules.[5,6] Nevertheless, only a few studies examined the mechanism and kinetics of fragmentation during emulsion preparation and how physical phenomena were modified by the use of stabilizers with more complex structures than molecular surfactants.

Theoretical approaches of emulsion formation have been proposed which were supported by experiments involving model systems either focusing on single droplets or rather dilute emulsions.[7–9]. In his pioneering work, Taylor investigated the deformation of a drop under flow and showed theoretically that the drop may burst provided that the capillary number (*Ca*, Eq. 1) exceeded a critical value, $Ca_{cr}$, which varied according to the viscosities of continuous and disperse liquid[7,8]

$$Ca = \frac{\dot{\gamma}\eta_c R_d}{\gamma_{ow}} \tag{1}$$

In Eq. 1, $\dot{\gamma}$ is the applied shear rate ($s^{-1}$), $\eta_c$ is the viscosity of the continuous phase (Pa s), $R_d$ is the droplet radius (m), and $\gamma_{ow}$ is the interfacial tension between the two phases (N $m^{-1}$).

Later the dependence of $Ca_{cr}$ on the viscosity ratio of disperse and continuous liquid phases ($p = \eta_d/\eta_c$) and type of flow was further investigated.[9] More recently, the kinetics and mechanism of fragmentation of an initial coarse emulsion into smaller droplets under defined shear stress was reported.[10] Nevertheless, there is still need for better understanding of the kinetics of emulsion formation starting from initially separated liquid phases, in concentrated conditions and under scalable experimental conditions.[11,12]

In a previous work, a new experimental rheo-optical device coupling shear stress and steady light transport measurements was introduced together with the theoretical derivations allowing data interpretation.[13,14]. One of the first

Additional Supporting Information may be found in the online version of this article.

[†]Pr. C. Baravian deceased at the end of year 2012. This article is dedicated to his memory.

Correspondence concerning this article should be addressed to A. Durand at Alain.Durand@univ-lorraine.fr.

Current address of Emmanuelle Marie: ENS – Département de Chimie, UMR 8640 CNRS – ENS – UPMC, 24 Rue Lhomond, Paris, F-75005, France

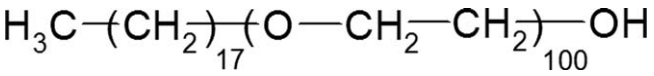

**Figure 1. Chemical structure of polymeric surfactant, Brij700®.**

applications of these results was a continuous *in situ* monitoring of global shear stress and average droplet diameter during emulsification under mechanical agitation and in concentrated conditions (50% oil volume fraction).[15] The overall kinetics of emulsion formation was described by dividing it into four successive steps. Initial flow start-up (first step) was followed by the formation of a coarse emulsion called "premix" (second step). Then, this coarse emulsion underwent a continuous droplet diameter reduction accompanied by an increase of shear stress (third step) which stopped at a well-defined time after which the final steady state of droplet diameter and viscosity was attained (fourth step or "stationary state").

Apart from emulsion formation, this original device may be a powerful tool for investigating the effect of stirring speed on nano-object morphology in reactive emulsion systems.[16–18]

In that work, we investigated the kinetics of oil-in-water emulsion formation under mechanical stirring in Couette geometry and focused our experiments on two physical variables, oil volume fraction in the feed, and applied shear rate. Hexadecane was the oil used for all experiments. As for the aqueous phase, a commercial nonionic amphiphilic polymer (Brij700®) was used as stabilizer and the viscosity level was adjusted by a commercial viscosifier ensuring a Newtonian rheological behavior. Experimental results were compared to theoretical predictions based on a physical model using equations from literature.

## Materials and Methods

### *Materials*

All chemicals were from Aldrich® and were used without further purification.

Aqueous phase was prepared as follows. Commercial surfactant, Brij700® (Figure 1) was weighted and dissolved in water at a concentration of 20 g $L^{-1}$ during 48 h under magnetic stirring. Sodium azide was added at a concentration of 20 mg $L^{-1}$. Afterward, Emkarox V45® was added at an amount of 25 wt % of aqueous phase. Refraction indices were experimentally determined at 25°C and were found equal to 1.35 for aqueous phase (prepared with Emkarox HV45®) and 1.46 for hexadecane. The viscosity of hexadecane was measured using cone-plate geometry and found equal to $3.45 \pm 0.1$ mPa s at 20°C. Interfacial tension between aqueous phase containing Brij700® and hexadecane was measured at 25°C using Krüss tensiometer with De Noüy platinum ring which was immersed at interface during 25 min. Three successive determinations were carried out every 20 min.

### *Experimental device and procedure*

The experimental device consisted in two parts: a rheometer (AR 2000® TA Instrument) and an optical part (Figure 2). The detailed description of the apparatus, vane geometry calibration procedure, and determination of average droplet radius had been given in previous publications.[13–15,19] Briefly, the measurement geometry used for rheometry was a six blade vane of 11-mm radius and an immersed height of 24 mm. This vane was centered inside a cylinder of 12.3-mm inner radius sealed onto a glass plate. Using the previously described protocol and several silicon oils of known viscosities, the shear stress and shear rate geometrical factors were determined.[19] The optical part of the apparatus consisted of a laser diode (wavelength = 635 nm), a circular polarizer to control incident polarization, a CCD camera as detector, and two mirrors. The position of laser impact at the bottom of the geometry corresponded to the center of a recirculation zone where there was an exchange between the sheared zone and the bottom of the geometry. Thus, size measurements were representative of the sheared region. The camera recorded the light backscattered by the sample yielding a $5 \times 5$ $mm^2$ image which represented the backscattered incoherent light transport far from the impact of the laser. The previous spatial intensity decrease was fitted by a steady-state radiative transfer model in the diffusion approximation which involved a single variable, the transport length.[13] Knowing the refractive index of oil and oil volume fraction allowed relating transport length to average droplet radius through Mie theory. Assuming that refractive index and oil volume fraction remained constant during emulsification implied that the variation of transport length was directly related to variation of average droplet radius.

The aqueous phase and hexadecane were initially added into the vane geometry and emulsification started with the rotation at a fixed speed. Shear stress and back-scattered intensity were registered regularly.

Independent determinations of average droplet radius were carried out with final emulsions using laser granulometry (Mastersizer 2000®, Malvern Instrument). For these measurements, samples were diluted in $10^{-3}$ M NaCl aqueous solution.

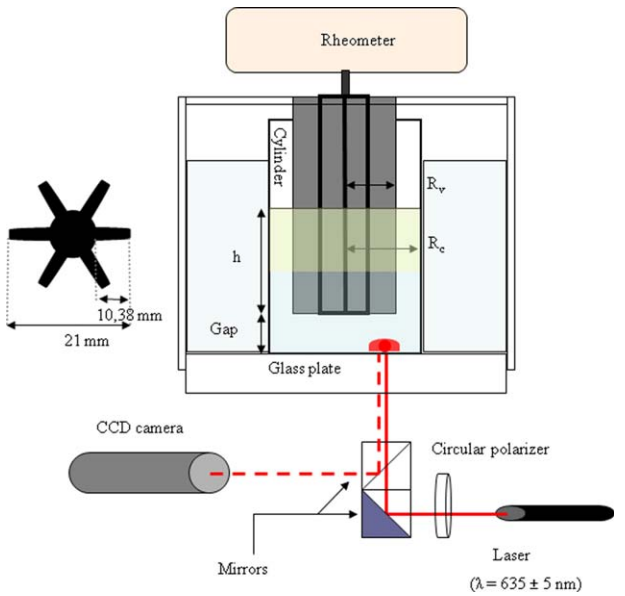


**Figure 2. Schematic representation of rheo-optic experimental device and vane geometry and dimensions (on left).**

**[Color figure can be viewed in the online issue, which is available at wileyonlinelibrary.com.]**

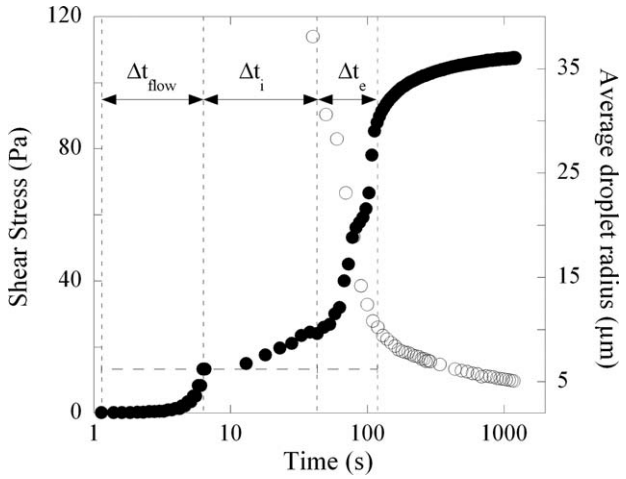


**Figure 3. Variation of shear stress (•) and average droplet radius (○) with time during emulsification with 50% v/v hexadecane at 70 rad $s^{-1}$.**

**Definitions of time of flow setup ($\Delta t_{flow}$), inertial time ($\Delta t_i$), and emulsification time ($\Delta t_e$).**

## Results and Discussion

### *Physico-chemical characteristics of selected systems*

Emulsification of hexadecane in water in the presence of a water-soluble commercial polymeric surfactant, Brij700® (Figure 1) was investigated. Because of the ultralow solubility of hexadecane in water and considering the range of droplet diameters (above 1 μm), any influence of molecular diffusion during emulsification was ignored.[20] The aqueous phase was a mixture of commercial Emkarox HV45® and water (25 and 75 wt %, respectively), in which Brij700® was dissolved at a concentration of 16 g $L^{-1}$. The viscosity of the aqueous phase at 20°C exhibited no significant variation with applied shear rate between 1 and 1000 $s^{-1}$ and the presence of Brij700® at the used concentration did not induce a significant modification (Supporting Information Figure 1S). The experimental value of viscosity was 88 mPa s.

Interfacial tension between aqueous phase and hexadecane was measured at 25°C in the presence of Brij700® at 16 g $L^{-1}$ and found equal to 15 mN $m^{-1}$. Oil-in-water emulsions were prepared with hexadecane volume fractions ranging between 10 and 60% v/v and under constant shear rates between 347 and 695 $s^{-1}$. The upper limit of shear rate was imposed by the characteristics of the rheometer. Independent characterizations of droplet size distributions were performed after sampling final emulsions, using laser granulometry. For all reported experiments, the average droplet radius calculated from the transport length was almost identical to the volume-average droplet radius obtained from laser granulometry as it had been demonstrated in a previous article.[15] It had been showed previously that for volume fractions higher than 70% v/v, the transport of light was significantly influenced by the Plateau borders between oil droplets and consequently, polarized light was related to distances between the droplets instead of their size.[21] Even if average droplet size could be determined using a geometrical model of dispersions, we preferred to avoid this aspect for focusing on fragmentation kinetics. Thus, we limited oil volume fraction to 60% v/v.

In a previous work, we determined experimentally that Brij700® adsorption at dodecane/water interface led to a surface coverage of 4 mg $m^{-2}$ at the maximum.[22] Taking this value as a good order of magnitude for hexadecane/water interface, we calculated that with 16 g $L^{-1}$ of Brij700® and 60% v/v of oil, the droplet radius corresponding to a complete adsorption of the added surfactant would be 1 μm. As all the measured values were higher than 1 μm, we considered that there was no limitation by the available amount of stabilizer. In addition, emulsions with different oil volume fractions between 10 and 40% v/v were characterized by laser granulometry immediately after emulsification and after 5-day storage at room temperature. Although creaming was detected visually in all samples, droplet diameter distributions determined after manual agitation were not significantly different from the initial ones. This result confirmed the efficient prevention of droplet coalescence by Brij700®. Consequently, we assumed that droplet radii were not controlled by coalescence but mainly by droplet fragmentation.

### *Experimental investigation of emulsification kinetics*

*Definition of Characteristic Time Periods.* For all experiments, the variation of shear stress and average droplet radius with time followed a typical curve (Figure 3) which allowed defining inertial time ($\Delta t_i$) and emulsification time ($\Delta t_e$).[15] An initial time period corresponded to the establishment of flow of biphasic mixture and its duration was noted $\Delta t_{flow}$.

The inertial time corresponded to the time necessary for the formation of a coarse emulsion (also called "premix") from the initial biphasic mixture in an established flow field. The inertial time was determined from the variation of global shear stress as the time interval between the setup of flow and the beginning of sharp increase of shear stress, which was interpreted as the beginning of droplet fragmentation. The first measurable average droplet radius value was obtained just after "premix" formation, which is another indication that the formation of small droplets started after the end of that period and took place by another mechanism involving shear forces (Figure 3).

The emulsification time was the time needed for fragmentation of droplets of "premix" so as to produce final micronic emulsions. It was determined from the variation of the global shear stress as the time interval between the beginning of shear stress increase and the time corresponding to 80% of the stationary value of shear stress. After the end of the emulsification period, both variations of shear stress and average droplet radius were much slower and finally reached the stationary state.

With the aim to get further insight into the process of droplet fragmentation, we examined how the kinetics of emulsification (characterized by $\Delta t_i$ and $\Delta t_e$) as well as the characteristics of formed emulsions (average droplet radius and viscosity) were influenced by the rotational speed and the oil volume fraction.

*Influence of Rotational Speed and Oil Volume Fraction.* In a first series of experiments, hexadecane-in-water emulsions were prepared keeping the same oil volume fraction (50%) and varying the rotational speed between 50 and 100 rad $s^{-1}$. No emulsification was observed with the lowest rotational speed (50 rad $s^{-1}$, Figure 4). For all other experiments, both characteristic times, $\Delta t_i$ and $\Delta t_e$, decreased when the rotational speed was increased. In particular, $\Delta t_i$ was of the order of some seconds for the highest rotational speeds (90 and 100 rad $s^{-1}$). As for the average droplet radius,

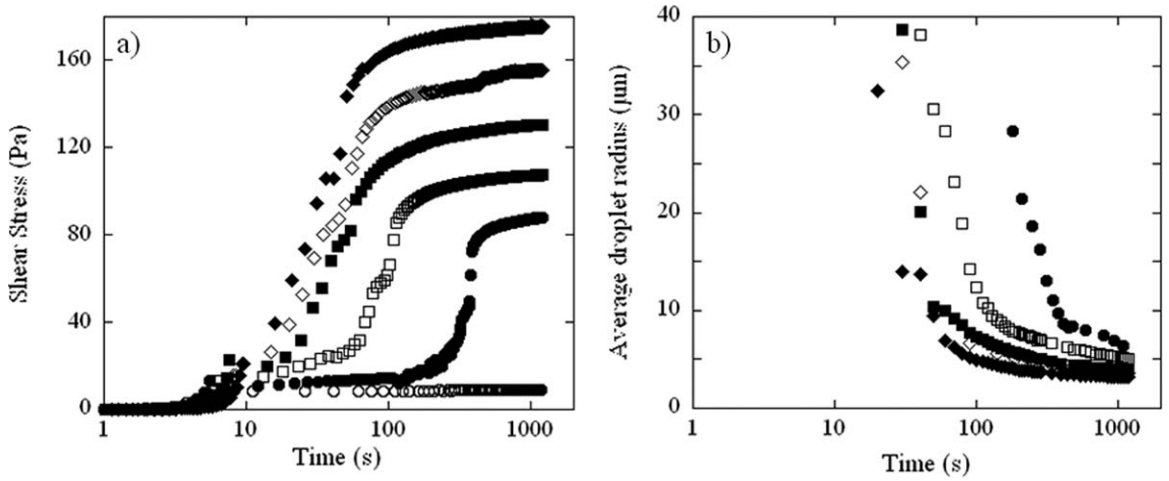


**Figure 4. Variation of shear stress (a) and average droplet radius (b) with time during emulsification with 50% v/v hexadecane and at various rotational speeds (○) 50 rad $s^{-1}$, (•) 60 rad $s^{-1}$, (□) 70 rad $s^{-1}$, (■) 80 rad $s^{-1}$, (⌑) 90 rad $s^{-1}$, and (◆) 100 rad $s^{-1}$.**

during the emulsification step, it decreased down to a minimum value (Figure 4). This minimum value was lowered at higher rotational speeds.

In a second series of experiments, rotational speed was kept at 100 rad $s^{-1}$ and the volume fraction of hexadecane was varied between 20 and 60%. Global shear stress variation as well as average droplet radius variation with time was similar over the whole range of oil volume fraction (Figure 5). Both characteristic times, $\Delta t_i$ and $\Delta t_e$, remained almost unchanged over the whole range of oil volume fractions. The final average droplet radius decreased when increasing oil volume fraction.

*Proposed Mechanism for Droplet Fragmentation.* ***First and second step: Flow establishment and formation of a coarse emulsion.*** All experiments started with a biphasic liquid mixtures. Thus, a first period of time was required to establish the flow of the two liquid phases. The duration of this initial period was always around 6 s.

During the following steps, the biphasic flow led to fragmentation of oily phase into droplets dispersed within the aqueous phase. The formation of an oil-in-water emulsion was consistent with the hydrophilic nature of Brij700® as indicated by its hydrophilic-lipophilic number equal to 18.[22]

The first measurable droplet radius was obtained at the end of this second step which was another indication that only after this second step an initial emulsion was obtained. Thus, after the setup of biphasic flow, the second step which lasted $\Delta t_i$ consisted in the formation of a coarse emulsion, that we called "premix." The average droplet radius of premix emulsions was between 20 and 40 μm except for the two highest oil volume fractions (55 and 60%) for which much higher values were obtained (up to 100 μm). It decreased slightly when the shear rate was increased. In a previous study, we showed that the viscosity of the aqueous phase had no significant effect on the average radius of premix droplets.[15]

We defined the Reynolds number of the flow using the characteristic dimensions of vane geometry (Eq. 2)

$$Re_{\text{flow}} = \frac{\Omega R_{\text{pale}} e}{\upsilon} \tag{2}$$

In Eq. 2, Ω is the rotational speed (rad $s^{-1}$), $R_{\text{pale}}$ is the radius of one pale of vane geometry (m), $e$ is the gap of vane geometry (m), and $\upsilon$ is the kinematic viscosity of the fluid ($m^2$ $s^{-1}$). Using the properties of both liquid phases, we found $Re_{\text{flow}}$ values equal to 25 (for aqueous phase) and

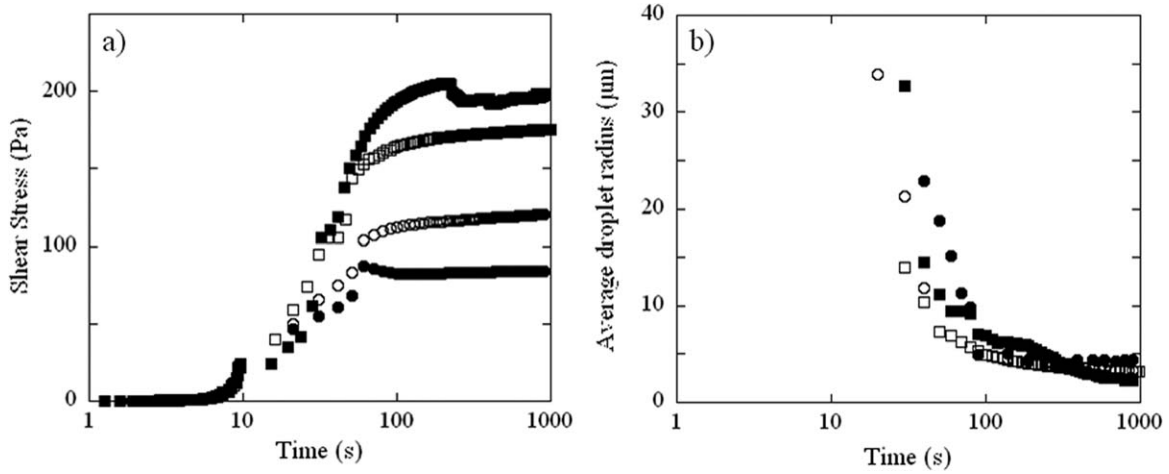


**Figure 5. Variation of shear stress (a) and average droplet radius (b) with time during emulsification of hexadecane at 100 rad $s^{-1}$ and with various oil volume fractions (•) 20%, (○) 40%, (□) 50%, and (■) 60%.**

**Table 1. Duration of Flow Establishment, Inertial and Emulsification Periods, Initial Capillary Number, Characteristic Frequency of Droplet Fragmentation (Eq. 5), and First-Order Rate Constant of Shear Stress Variation Determined for Different Experimental Conditions of Emulsion Preparation**

| Rotational Speed (rad $s^{-1}$) | Hexadecane Volume Fraction (%) | $\Delta t_{flow}$ (s) | $\Delta t_i$ (s) | $\Delta t_e$ (s) | $Ca^*_{ini}$ | $\omega_0$ ($s^{-1}$) | $k$ ($s^{-1}$) |
|---|---|---|---|---|---|---|---|
| 50 | 50 | 4.5 | – | – | – | – | – |
| 60 | 50 | 5.6 | 126 | 250 | 0.04 | 0.016 | 0.0049 |
| 70 | 50 | 6.3 | 37 | 75 | 0.06 | 0.018 | 0.0145 |
| 80 | 50 | 7.2 | 12 | 55 | 0.12 | 0.015 | 0.0242 |
| 90 | 50 | 8.1 | 3 | 54 | 0.16 | 0.011 | 0.0236 |
| 100 | 50 | 9.3 | 2 | 40 | 0.13 | 0.023 | 0.0302 |
| 100 | 20 | 9.3 | 1 | 41 | 0.09 | – | 0.0405 |
| 100 | 30 | 9.3 | 1 | 51 | 0.10 | – | 0.0325 |
| 100 | 40 | 9.3 | 1 | 51 | 0.11 | 0.013 | 0.0274 |
| 100 | 55 | 10.3 | 0 | 44 | 0.24 | 0.007 | 0.0304 |
| 100 | 60 | 9.6 | 5 | 43 | 0.26 | 0.007 | 0.0355 |

For details see text.

500 (for hexadecane). These values show that during the second step, between flow setup and premix formation, the flow regime may be intermediate and both shear and inertial stresses may be responsible for the value of initial average droplet diameter. Nevertheless, after the end of the second step, as overall viscosity increased significantly, the flow was laminar and further droplet breakup was caused by shear forces.

***Third step, laminar regime.*** During this third step, a significant decrease of average droplet radius was observed, associated with a strong increase of global shear stress. As demonstrated earlier, droplet rupture occurred by shear forces. Consequently, we used Capillary number as the relevant criterion. Nevertheless, the expression of Eq. 1 held for isolated drop while for droplet breakup in emulsions, it had been demonstrated that the properties of continuous phase should be replaced by those of the emulsion itself.[23,24] Thus we defined $Ca^*$ on the basis of global shear stress (Eq. 3)

$$Ca^* = \frac{\tau_{em} R_d}{\gamma_{ow}} \tag{3}$$

In Eq. 3 $\tau_{em}$ is the global shear stress undergone by emulsion (Pa) as measured by rheometer.

Using simultaneous measurements of average droplet radius and global shear stress, we estimated $Ca^*$ just after the beginning of the third step, that is, when the first radius value was obtained. This value was called the "initial capillary number" and noted $Ca^*_{ini}$. It appeared that the lowest $Ca^*_{ini}$ value corresponding to emulsification was about 0.04 (Table 1). Thus, on the basis of this series of experiments with increasing rotational speed, we concluded that in our conditions, $Ca^*_{cr}$ should be close to 0.04. This value corresponded to a viscosity ratio $p = \eta_d/\eta_c$ equal to 0.04 and was consistent with the value of 0.1 reported previously for $p = 1$ also for non quasistatic conditions.[10]

During this third step, the variation of average droplet radius with time could be separated in two regimes.

During the first 20 s, droplet radius decreased from about 40 μm down to 10–15 μm. Afterward, droplet radius was further reduced down to 1–6 μm over much longer time periods (between 100 and 1000 s). These two regimes of droplet fragmentation had been observed by other authors.[10,25,26] It was showed by microscope observations that the first regime involved deformation of drops into long cylinders which broke into aligned droplets (Rayleigh instability).[10]

During the second regime, droplet fragmentation occurred by a different mechanism with a much longer characteristic time. In the case of dilute oil-in-water emulsions (2.5 wt % of oil) submitted to a constant shear rate, the kinetics of fragmentation has been studied by analyzing samples after various shearing times.[10] The authors proposed to consider that, during this period, each oil droplet was broken into $(\omega + 1)$ smaller droplets per unit time. As droplet radius reached an asymptotic value, $\omega$ should be a function of droplet radius $\omega(R_d)$ which canceled for any value equal to or lower than the asymptotic value. A simple function was postulated to describe this dependence of $\omega$ (Eq. 4)[10]

$$\omega = \omega_0 \frac{R_d - R_f}{R_f} \text{ for } R_d > R_f \text{ and } w = 0 \text{ for } R_d < R_f \tag{4}$$

In Eq. 4, $R_0$ and $R_f$ are initial and final (asymptotic) average droplet radii (m), respectively, and $\omega_0$ is a characteristic frequency of droplet fragmentation ($s^{-1}$). Combining Eq. 4 with the condition of oil volume conservation allowed deriving the time variation of droplet radius during fragmentation under shear (Eq. 5, complete derivation available in Supporting Information)

$$R_d(t) = \frac{R_f}{1 - \frac{R_0 - R_f}{R_0} \exp\left(-\frac{\omega_0 t}{3}\right)} \tag{5}$$

*In situ* monitoring of average droplet radius provided experimental value of $R_d(t)$, $R_0$, and $R_f$ under defined conditions of droplet fragmentation. Thus, calculated variations obtained by Eq. 5 were fitted to experimental values and $\omega_0$ was the only adjustable parameter. Experimental variations of droplet radius were correctly described (Figure 6) and the found values of $\omega_0$ were between 0.007 and 0.023 $s^{-1}$ for all tested conditions (Table 1).

To the best of our knowledge, only two studies reported quantitative comparisons between experimental fragmentation kinetics and the variation predicted by Eq. 5.[10,25] Mabille et al. reported a value of 0.015 $s^{-1}$ for $\omega_0$, that is, of the same order of magnitude as for our experiments, but for much more dilute emulsions (2.5 wt % oil). In the case of emulsification in a two-rod batch mixer with oil/water mixtures containing 91.6 wt % oil, other authors also found a correct fit and reported values of $\omega_0$ around 0.004 $s^{-1}$ for various rotational speeds.[25] For both studies, $\omega_0$ values were obtained on the basis of a limited number of experimental

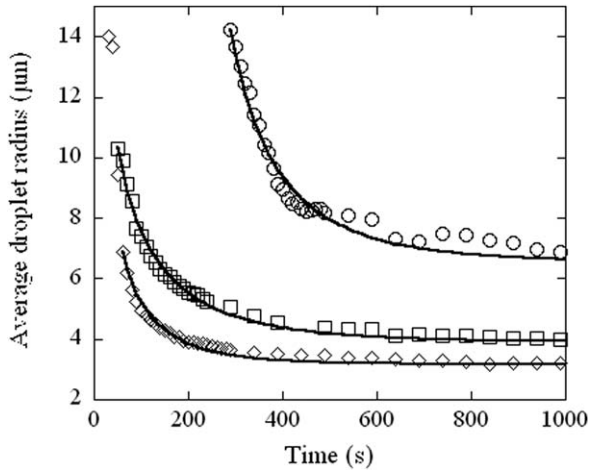


**Figure 6. Curve fitting of experimental variation of average droplet radius during emulsification period using Eq. 5.**

**Mixtures contained 50% v/v hexadecane and rotational speed was 60 rad $s^{-1}$ (○), 80 rad $s^{-1}$ (□), and 100 rad $s^{-1}$ (◇).**

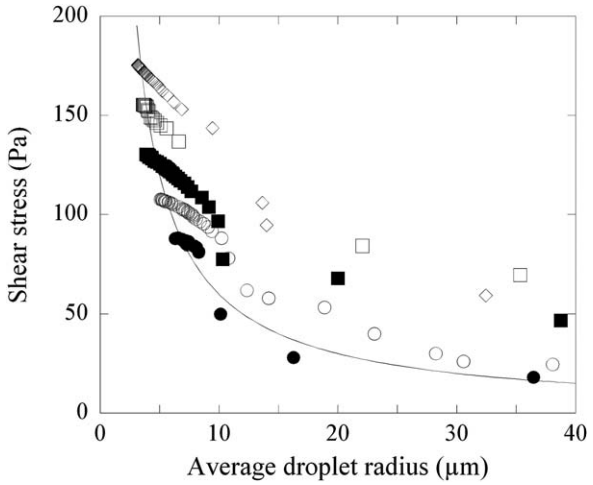


**Figure 7. Variation of shear stress with average droplet radius during droplet fragmentation under laminar regime with 50% v/v hexadecane and various rotational speeds (○) 60 rad $s^{-1}$, (•) 70 rad $s^{-1}$, (□) 80 rad $s^{-1}$, (■) 90 rad $s^{-1}$, and (◇) 100 rad $s^{-1}$.**

**The line is the calculated curve assuming that *Ca** remains equal to 0.04 (for details see text).**

points and radius variations within narrow intervals (2–5 μm).

We observed no significant variation of $\omega_0$ with rotational speed or with oil volume fraction (between 20 and 60% v/v oil). In addition, both regimes were observed in all experiments.

Apart from the variation of droplet radius with time, some authors also investigated the variation of mechanical stress during emulsification. In the case of emulsification with controlled rotational speed (between 100 and 300 rpm) mixing rheometer using an anchor impeller, a first-order kinetic equation was proposed to depict the variation of torque during the formation of oil-in-water emulsions containing 75 wt % oil.[27] When using a first-order kinetic equation for depicting the variation of shear stress within the third period, we obtained correct agreement only for rotational speeds higher than 80 rad $s^{-1}$ (764 rpm) and oil volume fractions above 30% (Supporting Information Figure 2S). The corresponding characteristic rate constants $k$ were between 0.02 and 0.04 $s^{-1}$ according to rotational speed and oil volume fraction (Table 1), that is, in the same range as in this previous study. As the geometry was significantly different (anchor impeller) no further comparison was attempted.

Taking the opportunity of our experimental setup coupling rheometry and droplet radius *in situ* measurements, we plotted the variation of shear stress with average droplet radius during droplet fragmentation under laminar regime (Figure 7). For the lowest rotational speeds, experimental points were very close to the curve calculated assuming that the $Ca^*$ remained equal to $Ca^*_{cr}$ during the whole droplet fragmentation period. This appeared consistent with our previous discussions showing that for these two rotational speeds the values of $Ca^*_{ini}$ were very close to 0.04 (Table 1). On the contrary, for other conditions, experimental points were in the vicinity of the calculated curve only at the end of the third period, that is, when the minimum attainable droplet radius was reached.

***Viscosity and droplet radius reached in the fourth step, stationary state.*** When plotting the final average droplet radius as a function of the final shear stress, all experimental points (different rotational speeds and different oil volume fractions) grouped into a master curve (Figure 8). Assuming that droplet rupture occurred by shear forces in laminar regime, the final droplet radius should be imposed by the value of $Ca^*_{cr}$.[28] On the basis of data obtained within the third period, we estimated that $Ca^*_{cr}$ was close to 0.04. Using Eq. 3 and $Ca^*_{cr} = 0.032$, we obtained a calculated curve which satisfactorily depicted experimental values (Figure 8) showing that the data of the stationary state were fully consistent with the fragmentation mechanism proposed.

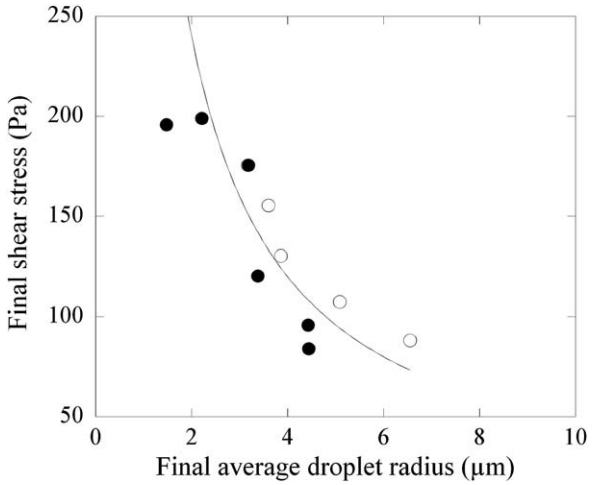


**Figure 8. Final average droplet radius as a function of the final shear stress, for all experimental conditions: different rotational speeds at 50% v/v hexadecane (open circles) and different oil volume fractions at 100 rad $s^{-1}$(bold circles).**

**The line represents theoretical variation assuming that *Ca** remains equal to 0.032 (for details see text).**

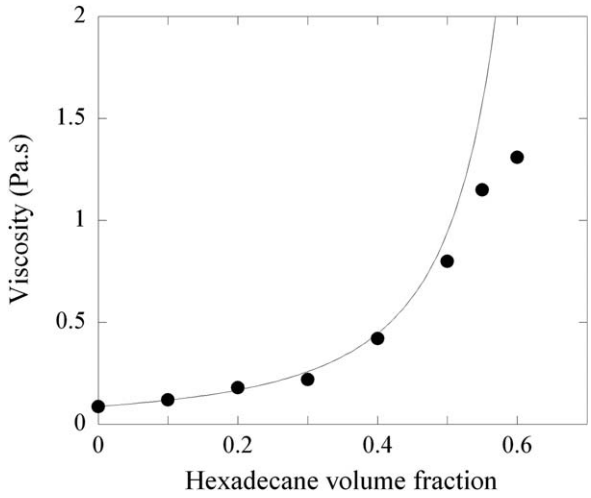


**Figure 9. Final emulsion viscosity as a function of oil volume fraction for all experimental conditions.**

**The line represents the theoretical curve given by Quemada's equation for hard spheres with a maximum packing volume fraction equal to 0.72 (for details see text).**

As the stationary average droplet radius corresponded to the minimal size to be fragmented, during the fourth step mechanical energy should be totally dissipated by viscosity. Final emulsion viscosity was plotted as a function of oil volume fraction (Figure 9). We tried to depict the experimental points using the expression derived by Quemada for suspensions of hard spheres[29] (Eq. 6)

$$\eta_{em} = \eta_c \left(1 - \frac{\phi}{\phi_m}\right)^{-2} \quad (6)$$

In Eq. 6, $\eta_{em}$ is emulsion viscosity (Pa s), $\phi$ is oil volume fraction, and $\phi_m$ is the maximum packing volume fraction.

The model of hard spheres described correctly experimental points with a maximum packing volume fraction equal to 0.72 (Figure 9). This value was fully consistent with previous results about flow of suspensions of monodisperse hard spheres.[30]

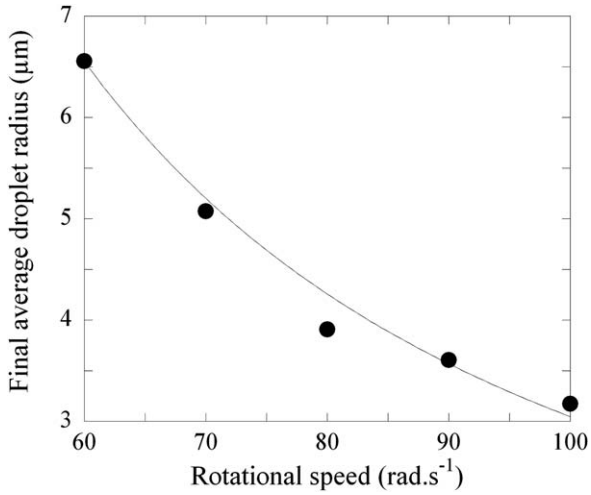


**Figure 10. Variation of final average droplet radius with rotational speed, with 50% oil volume fraction.**

**The line represents a power equation with an exponent equal to −3/2.**

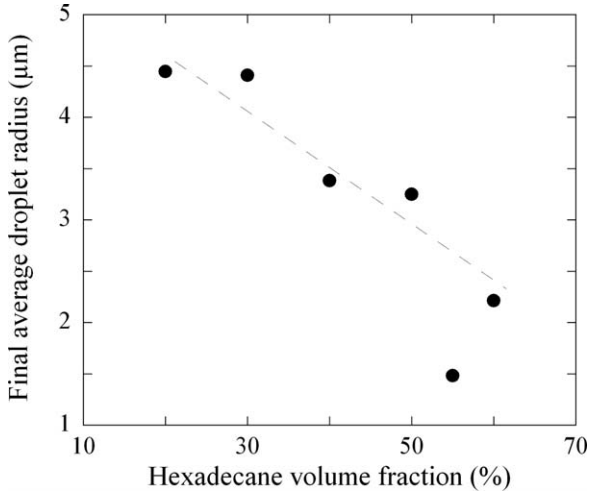


**Figure 11. Variation of final average droplet radius with oil volume fraction at 100 rad $s^{-1}$.**

**The line is a guide for the eye.**

We examined how the two operational parameters selected in that work, oil volume fraction and rotational speed, affected the final average droplet radius. The final droplet radius decreased with increasing rotational speed, with the experimental relation $R_f \propto \Omega^{-3/2}$ (Figure 10). This effect or rotational speed was explained by the increase of shear forces. In addition, the final radius decreased slightly with increasing oil volume fraction following an almost linear variation (Figure 11). This effect is consistent with higher emulsion viscosities at higher oil volume fractions which in turn induce higher shear forces at a constant rotational speed.

## Conclusion

The use of simultaneous *in situ* measurements of average droplet radius and global shear stress appeared as a powerful technique for investigating the kinetics of formation of oil-in-water emulsions stabilized by a nonionic surfactant in Couette geometry. On the basis of experimental data, the mechanism and kinetics of droplet fragmentation were analyzed and depicted with semiquantitative equations adapted from literature. We particularly investigated the effects of rotational speed and oil volume fraction on the kinetics and properties of final emulsions. Rotational speed was the most influent parameter. On the contrary, the effect of oil volume fraction between 20 and 60% v/v was less significant: no effect on the kinetics and a limited effect on the final droplet radius.

This work illustrated the interest of coupled *in situ* measurements covering two scales of matter: macroscopic scale (rheology) and microscopic scale (oil droplets). These experiments provided data for physical description of phenomena and information for scaling up the process. Starting from these results, we are currently continuing this work in two directions. First, we replace the nonionic surfactant and the viscosifier by macromolecules based on polysaccharides to examine the effect of structural complexity and non-Newtonian behavior on kinetics of fragmentation and characteristics of final emulsions. Second, we would like to apply

the coupling of *in situ* rheology and droplet radius measurements as a tool to monitor systems in which transient structures may be formed under defined shears forces so as to be able to obtained new types of colloids by scalable processes.

## Notation

$Ca$ = capillary number for an isolated droplet
$Ca^*$ = capillary number for an emulsion
$Ca_{cr}$ = critical capillary number for an isolated droplet
$Ca^*_{cr}$ = critical capillary number for an emulsion
$Ca^*_{ini}$ = capillary number at the beginning of emulsification
$e$ = gap of vane geometry, m
$k$ = first-order rate constants, $s^{-1}$
$p$ = ratio of disperse phase viscosity to continuous phase viscosity
$R_d$ = average droplet radius, m
$R_0$ = initial average droplet radius, m
$R_f$ = final (asymptotic) average droplet radius, m
$R_{pale}$ = radius of one pale of vane geometry, m
$Re_{flow}$ = Reynolds number defined for vane geometry
$t$ = time, s

### *Greek letters*

$\Delta t_e$ = emulsification time, s
$\Delta t_{flow}$ = time for flow establishment, s
$\Delta t_i$ = inertial time, s
$\phi$ = oil volume fraction
$\phi_m$ = maximum packing volume fraction
$\gamma_{ow}$ = oil water interfacial tension, N $m^{-1}$
$\dot{\gamma}$ = shear rate, $s^{-1}$
$\eta_c$ = viscosity of continuous phase, Pa s
$\eta_d$ = viscosity of disperse phase, Pa s
$\eta_{em}$ = emulsion viscosity, Pa s
$\upsilon$ = kinematic viscosity, $m^2$ $s^{-1}$
$\tau_{em}$ = global shear stress applied to emulsion, Pa
$\Omega$ = rotational speed, rad $s^{-1}$
$\omega$ = instantaneous frequency of droplet fragmentation, $s^{-1}$
$\omega_0$ = characteristic frequency of droplet fragmentation, $s^{-1}$

## Literature Cited


1. Charpentier JC. The triplet "molecular processes-products-process" engineering: the future of chemical engineering? *Chem Eng Sci*. 2002;57:4667–4690.
2. Charpentier JC. Among the trends for a modern chemical engineering, the third paradigm: the time and length multiscale approach as an efficient tool for process intensification and product design and engineering. *Chem Eng Res Des*. 2010;88:248–254.
3. Hill M. Product and process design for structured products. *AIChE J*. 2004;50:1656–1661.
4. Wibowo C, Ng KM. Product-centered processing: manufacture of chemical-based consumer products. *AIChE J*. 2002;48:1212–1230.
5. Tadros TF. Polymeric surfactants in disperse systems. *Adv Colloid Interface Sci*. 2009;147–148:281–299.
6. Tadros TF. Principles of emulsion stabilization with special reference to polymeric surfactants. *J Cosmet Sci*. 2004;55:406–407.
7. Taylor GI. The viscosity of a fluid containing small drops of another fluid. *Proc R Soc A*. 1932;138:41–48.
8. Taylor GI. The formation of emulsions in definable fields of flow. *Proc R Soc A*. 1934;146:501–523.
9. Grace HP. Dispersion phenomena in high viscosity immiscible fluid systems and application of static mixers as dispersion devices in such systems. *Chem Eng Commun*. 1982;14:225–277.
10. Mabille C, Leal-Calderon F, Bibette J, Schmitt V. Monodisperse fragmentation in emulsions: mechanism and kinetics. *Europhys Lett*. 2003;61:708–714.
11. Foerster T. Principles of emulsion formation. *Surf Sci Ser*. 1997;68:105–125.
12. Walstra P. Principles of emulsion formation. *Chem Eng Sci*. 1993;48:333–349.
13. Baravian C, Caton F, Dillet J, Mougel J. Steady light transport under flow: characterization of evolving dense random media. *Phys Rev E*. 2005;71:066603.
14. Baravian C, Caton F, Dillet J. Steady light diffusion application to rheology: a new tool for the characterization of concentrated suspensions. *Rheol Acta*. 2004;43:427–432.
15. Baravian C, Mougel J, Caton F, Durand A. Characterization of dynamical emulsification process in concentrated conditions. *AIChE J*. 2007;53:1994–2000.
16. Boissé S, Rieger J, Pembouong G, Beaunier P, Charleux B. Influence of the stirring speed and $CaCl_2$ concentration on the nano-object morphologies obtained via RAFT-mediated aqueous emulsion polymerization in the presence of a water-soluble macroRAFT agent. *J Polym Sci Part A: Polym Chem*. 2011;49:3346–3354.
17. Vauthier C, Bouchemal K. Methods for the preparation and manufacture of polymeric nanoparticles. *Pharm Res*. 2009;26:1025–1058.
18. Bourgeat-Lami E, Farzi GA, David L, Putaux J-L, McKenna TFL. Silica encapsulation by miniemulsion polymerization: distribution and localization of the silica particles in droplets and latex particles. *Langmuir*. 2012;28:6021–6031.
19. Baravian C, Lalante A, Parker A. Vane rheometry with a large, finite gap. *Appl Rheol*. 2002;12:81–87.
20. Sakai T, Kamogawa K, Nishiyama K, Sakai H, Abe M. Molecular diffusion of oil/water emulsions in surfactant-free conditions. *Langmuir*. 2002;18:1985–1990.
21. Paruta-Tuarez E, Fersadou H, Sadtler V, Marchal P, Choplin L, Baravian C, Castel C. Highly concentrated emulsions: 1. Average drop size determination by analysis of incoherent polarized steady light transport. *J Colloid Interface Sci*. 2010;346:136–142.
22. Wu M, Dellacherie E, Durand A, Marie E. Poly(n-butyl cyanoacrylate) nanoparticles via miniemulsion polymerization. 2. PEG-based surfactants. *Colloids Surf B*. 2009;69:147–151.
23. Jansen KMB, Agterof WGM, Mellema J. Droplet breakup in concentrated emulsions. *J Rheol*. 2001;45:227–236.
24. Tcholakova S, Lesov I, Golemanov K, Denkov ND, Judat S, Engel R, Danner T. Efficient emulsification of viscous oils at high drop volume fraction. *Langmuir*. 2011;27:14783–14796.
25. Caubet S, Le Guer Y, Grassl B, El Omari K, Normandin E. A low-energy emulsification batch mixer for concentrated oil-in-water emulsions. *AIChE J*. 2011;57:27–39.
26. Fournanty S, Le Guer Y, El Omari K, Dejean JP. Laminar flow emulsification process to control the viscosity reduction of heavy crude oils. *J Dispers Sci Technol*. 2008;29:1355–1366.
27. Sanchez MC, Berjano M, Guerrero A, Gallegos C. Emulsification rheokinetics of nonionic surfactant stabilized oil-in-water emulsions. *Langmuir*. 2001;17:5410–5416.
28. Walsta P, Smulders I. Making emulsions and foams: an overview. *RSC Spec Publ Food Colloids*. 1997;192:367–381.
29. Quemada D. Rheology of concentrated disperse systems and minimum energy dissipation principle 1. Viscosity-concentration relationship. *Rheol Acta*. 1977;16:82–94.
30. Jones DAR, Leary B, Boger DV. The rheology of a concentrated colloidal suspension of hard spheres. *J Colloid Interface Sci*. 1991;147:479–495.


*Manuscript received May 2, 2014, and revision received Aug. 24, 2014.*